

Frequency Adaptive Virtual Variable Sampling-based Selective Harmonic Repetitive Control of Power Inverters

Liu, Zhichao; Zhou, Keliang; Yang, Y.; Wang, Jingcheng; Zhang, Bin

Published in:
IEEE Transactions on Industrial Electronics

DOI (link to publication from Publisher):
[10.1109/TIE.2020.3031452](https://doi.org/10.1109/TIE.2020.3031452)

Publication date:
2021

Document Version
Accepted author manuscript, peer reviewed version

[Link to publication from Aalborg University](#)

Citation for published version (APA):
Liu, Z., Zhou, K., Yang, Y., Wang, J., & Zhang, B. (2021). Frequency Adaptive Virtual Variable Sampling-based Selective Harmonic Repetitive Control of Power Inverters. *IEEE Transactions on Industrial Electronics*, 68(11), 11339-11347. Article 9239879. <https://doi.org/10.1109/TIE.2020.3031452>

General rights

Copyright and moral rights for the publications made accessible in the public portal are retained by the authors and/or other copyright owners and it is a condition of accessing publications that users recognise and abide by the legal requirements associated with these rights.

- Users may download and print one copy of any publication from the public portal for the purpose of private study or research.
- You may not further distribute the material or use it for any profit-making activity or commercial gain
- You may freely distribute the URL identifying the publication in the public portal -

Take down policy

If you believe that this document breaches copyright please contact us at vbn@aub.aau.dk providing details, and we will remove access to the work immediately and investigate your claim.

Frequency Adaptive Virtual Variable Sampling-based Selective Harmonic Repetitive Control of Power Inverters

Zhichao Liu, *Student Member, IEEE*, Bin Zhang, *Senior Member, IEEE*,
Keliang Zhou, *Senior Member, IEEE*, Yongheng Yang, *Senior Member, IEEE*, and Jingcheng Wang

Abstract—Due to the n -pulse commutation, the power harmonic distortions caused by power inverters usually concentrate on particular $(nk \pm m)$ -order harmonic frequencies. The conventional repetitive control (RC) uses an identical gain to equally compensate for the distortions at all harmonic frequencies. This leads to slow dynamics as it fails to optimize the convergence rate of the RC at dominant harmonic frequencies. The selective harmonic RC (SHRC) can efficiently suppress dominant power harmonic distortions. However, the ratio of the sampling rate of the SHRC to the fundamental frequency must be an integer. This severely limits the use and lowers the performance of the SHRC with a fixed sampling rate in the presence of frequency variations of interested harmonics. To address this problem, this paper proposes a frequency adaptive virtual variable sampling-based SHRC (FA-VVS-SHRC) scheme that is immune to the issue of the fractional ratio of the sampling rate to the interested harmonics. The proposed FA-VVS-SHRC scheme can provide flexible fractional phase lead compensation to achieve accurate power harmonic control in the presence of frequency variations. Moreover, it is a low-cost and easy-to-implement solution that does not require hardware modifications. Experiments on a three-phase power inverter and comparison studies are presented to verify its effectiveness.

Index Terms—DC/AC inverter, frequency fluctuation, repetitive control, selective harmonics, virtual variable sampling

I. INTRODUCTION

IN electrical power systems, harmonics caused by power converter commutations usually concentrate on particular $(nk \pm m)$ -order harmonic frequencies with n being the pulse number of the power converter, $m < n$, and $k = 1, 2, \dots$. For instance, the harmonic frequencies of single-phase H-bridge inverters are mainly $4k \pm 1$ times of the fundamental frequency, while distortions of three-phase two-level inverters are typical $(6k \pm 1)$ -order harmonics [1]–[8]. To deal with these particular harmonics, selective harmonic repetitive control (SHRC) schemes were developed [9]. The SHRC can effectively and

accurately compensate for harmonics and, at the same time, maintain fast dynamics and strong robustness.

The SHRC scheme is typically implemented in digital signal processors with a period delay unit, $z^{-N/n}$, where N is the number of sample points in one reference fundamental signal period ($N = f_s/f_r$, f_s is the sampling frequency and f_r is the reference signal frequency) [10]. For digital control systems, the delay length N/n must be an integer, i.e., the sampling frequency f_s has to be an integral multiple of $f_r \times n$. This requirement, however, often does not hold in practical applications due to the following reasons: (1) The sampling frequency is not an integral multiple of $f_r \times n$. For example, a 60-Hz reference signal with a 10-kHz sampling frequency requires the period delay unit of $z^{-N/n} = z^{-27.78}$ to implement the SHRC in order to compensate for the dominant harmonics of 6-pulse converters, which is unachievable in DSPs or very difficult to do. (2) For grid-connected applications, the grid frequency always varies due to the power imbalance between the generation and load demands [11]–[13]. With a fixed sampling frequency of 10 kHz for 6-pulse converters, if the grid frequency fluctuates from 59.5 Hz to 60.5 Hz, the delay length N/n will correspondingly vary from 27.55 to 28.01. The fractional delay length N/n will degrade the harmonic suppression and deteriorate the output performance of SHRC, as N/n is usually approximated as an integer. Moreover, the employment of a fixed sampling frequency also leads to poor portability of the controllers. That is, the SHRC schemes designed for a 50-Hz system cannot universally be used in 60-Hz systems, as the control accuracy cannot be maintained.

To address this issue, variable sampling frequency schemes provide a general and intuitive solution that can achieve a constant integer ratio of N/n in the presence of frequency variations [14]–[17]. However, variable sampling methods not only require DSP's special variable sampling programming capacity but also need to recalculate or re-tune other digital control parameters to maintain the system stability and robustness [18], [19]. For example, in LCL-filtered systems, the active damping is closely related to the sampling frequency. It, in turn, increases the system cost and complexity.

Recently, the virtual delay unit concept was developed [16], [17], [20], which enables the virtual variable sampling (VVS) control. As an emerging technique, the VVS has some limitations that should be addressed. One major limitation is its performance degradation under frequency fluctuations. To tackle this problem, the virtual delay unit in [20] approximates the fractional delay due to frequency variations based a linear interpolation method, which requires heavy computation for a large number of delays and it is only suitable for a limited range of frequency mismatches. Accordingly, this paper

Manuscript received May 1, 2020; revised July 18 and September 03, 2020; accepted September 22, 2020. (Corresponding author: Bin Zhang.) This work is supported by Aspire of the University of South Carolina, National Natural Science Foundation of China (No.61533013, 61633019), and Shaanxi Provincial Key Project (2018ZDXM-GY-168).

Z. Liu and B. Zhang are with the Department of Electrical Engineering, University of South Carolina, Columbia, SC 29205 USA (e-mail: zhichao@email.sc.edu; zhangbin@cec.sc.edu)

K. Zhou is with the School of Automation, Wuhan University of Technology, China (e-mail: keliang.zhou@whut.edu.cn).

Y. Yang is with the Department of Energy Technology, Aalborg University, Denmark (email: yoy@et.aau.dk)

J. Wang is with Shanghai Jiaotong University and Xi'an Technological University (email: jcwang@sjtu.edu.cn)

extends the VVS control and proposes a frequency adaptive VVS-based SHRC (FA-VVS-SHRC) scheme to enable a low-cost and flexible solution. Different from the prior-art VVS methods, the FA-VVS-SHRC scheme accommodates frequency fluctuations by replacing fixed sampling period delays with virtual variable sampling period delays. By doing so, the FA-VVS-SHRC can accurately compensate for power harmonics distortions in the presence of a fractional ratio of N/n due to the fundamental frequency variations and/or the hardware limitations. It thus provides a generic and robust solution to the fractional delay unit issue of digital RC schemes [16], [20]. Experiments on a three-phase pulse width modulation (PWM) inverter (i.e., a 6-pulse inverter) are presented to demonstrate the effectiveness of the proposed method in dealing with frequency fluctuations.

The remainder of this paper is organized as follows: Section II introduces the conventional RC, the SHRC, and more importantly, proposes the FA-VVS-SHRC scheme. Experimental verification is performed on a three-phase PWM inverter, and the results are compared with conventional control methods in Section III. Concluding remarks are provided in Section IV.

II. FREQUENCY ADAPTIVE VVS-SHRC

A. Conventional RC

Fig. 1 illustrates the conventional RC (CRC) [21] with a plug-in structure, in which $R(z)$ is the periodic reference input, $G_c(z)$ is the feedback controller, $Y(z)$ is the system output, $G_p(z)$ is the plant model, and $D(z)$ is the disturbance. As shown in Fig. 1, the CRC scheme is a feed-forward controller that consists of an RC gain K_r , a low pass filter $Q(z)$, a phase lead filter $G_f(z)$, and a period delay z^{-N} . Let f_r and $T_r = 1/f_r$ denote the reference fundamental frequency and period of $R(z)$, and f_s and $T_s = 1/f_s$ be the system sampling frequency and period, respectively. Then, the number of sampling points in one reference signal period of $R(z)$ is calculated as $N = f_s/f_r = T_r/T_s$. In most existing RC designs, N must strictly be an integer. According to Fig. 1, the transfer function of the plug-in CRC $G_{RC}(z)$ is expressed as

$$G_{RC}(z) = \frac{U_r(z)}{E(z)} = K_r \frac{z^{-N}Q(z)}{1 - z^{-N}Q(z)} G_f(z) \quad (1)$$

where $E(z) = R(z) - Y(z)$ is the system tracking error.

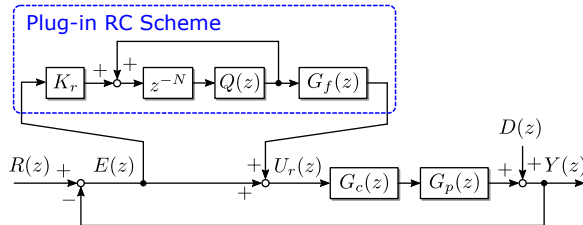


Fig. 1: Control system with the plug-in RC scheme.

A frequency domain analysis can be applied to Eq. (1), which shows that, when the low-pass filter $Q(z)$ is not considered, the CRC presents infinite magnitude gains at the fundamental and all harmonic frequencies of the reference signal. This means that, theoretically, the CRC can achieve

zero tracking error on the desired frequency and higher order harmonic components to achieve zero total harmonic distortion (THD).

B. Digital Selective Harmonic RC

As mentioned previously, the harmonics of power inverters usually concentrate on $nk \pm 1$ ($k = 0, 1, 2, \dots$) order frequencies. Based on the internal model principle, a universal selective harmonic compensation module that includes only the internal models of $(nk \pm m)$ -order harmonics can be designed. Fig. 2 shows the selective harmonic compensation module, which is tailored for the $(nk \pm m)$ -order harmonics, will achieve perfect compensation of the harmonics at the selective frequencies.

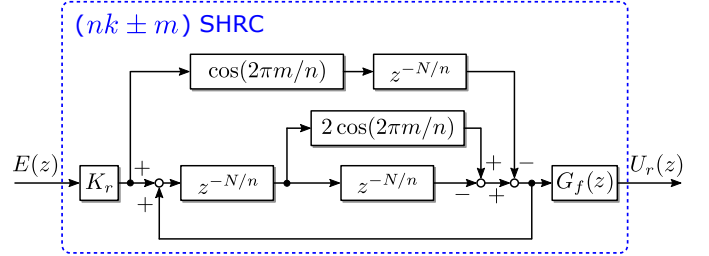


Fig. 2: Digital selective harmonic RC scheme.

The transfer function of the SHRC is given as

$$G_{SHRC}(z) = K_r \frac{\cos(2\pi m/n)z^{-N/n} - z^{-2N/n}}{1 - 2\cos(2\pi m/n)z^{-N/n} + z^{-2N/n}} \quad (2)$$

where $n, m \in \mathbb{N}$, $n > m \geq 0$. Since $G_{SHRC}(z)$ has infinite magnitudes at $(nk \pm m)$ -order frequencies, it can achieve zero tracking error at these harmonic frequencies, as aforementioned. More importantly, the design shown in Fig. 2 provides a flexible realization of the SHRC for different inverter topologies. For example, let $n = 1$ and $m = 0$, it is the CRC scheme, and let $n = 4$ and $m = 1$, it becomes an odd-order harmonic RC scheme for single-phase inverters [9]. More can be easily constructed by paralleling the SHRC modules.

C. Frequency Adaptation of SHRC

Similarly, the SHRC scheme requires the ratio of $N/n = T_r/T_s$ be an integer such that the internal models in the SHRC controller can well match the power harmonics. However, when the sampling period T_s does not meet the requirement and/or the reference signal's period T_r has fluctuations, the sampling points between two cycles of the reference signal will not be in the same phase. This means that the internal models in the RC mismatch the signals of interest. To further explain this issue, Fig. 3 illustrates the scenario when the reference signal's period T_r fluctuates under a constant sampling period of nT_s . As observed in Fig. 3, when the reference signal's period deviates from T_r to \hat{T}_r , the sampling points in the period of \hat{T}_r are not in the same phase with those in the period of T_r . This phase mismatch will severely degrade the RC's performance, including the SHRC, and even lead to system instability. Hence, it is necessary to develop frequency adaptive schemes to ensure the harmonic compensation performance.

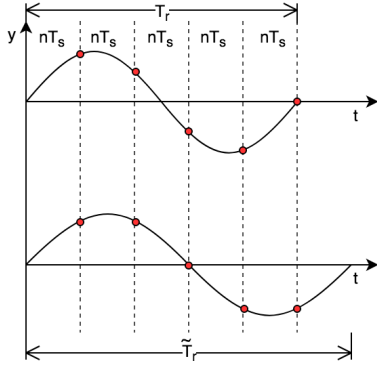


Fig. 3: Illustration of the performance degradation of the RC schemes with a constant sampling period nT_s when the reference signal frequency T_r varies.

D. Virtual Variable Sampling

To avoid the phase mismatch of sampling points under frequency fluctuation, the frequency adaptive RC requires a fixed sampling point number in one reference period under a varying reference frequency. When the reference period changes, the sampling period is adjusted accordingly to maintain the fixed sampling number, as illustrated in Fig. 4. That is, the variable sampling period \tilde{T}_r should meet the following requirement:

$$\tilde{T}_s = \tilde{T}_r / (n \cdot N) \quad (3)$$

where \tilde{T}_r is the variable reference signal period, n is the ratio from selective $(nk \pm m)$ -order harmonics, and N is the number of sampling points in the RC.

The variable sampling period can be achieved by hardware modification. However, there are some limitations: 1), it requires particular DSP processing capacity that will increase the hardware cost; and 2), the hardware variable sampling period affects not only the RC scheme itself but also the conventional feedback controller $G_c(z)$, as aforementioned. The variable sampling period also needs to consider the influence on the stability of the conventional control loop.

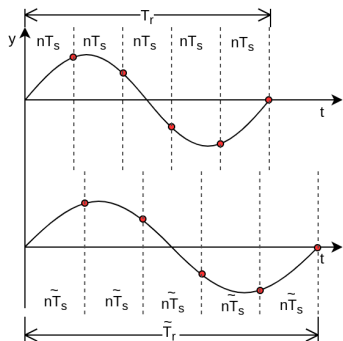


Fig. 4: Adaptive sampling period under T_r fluctuation.

These limitations can be overcome by the VVS technique, which employs fixed sampling period delays to approximate a variable sampling period delay in the control system. Fig. 5 exemplifies a 3-sampling-point VVS, which is based on the three sampling points at the time instants of $-T_s$, $-2T_s$, and $-3T_s$, and the approximation range is between $-T_s$

and $-3T_s$. By constructing a polynomial through the three sampling points, the approximation can be calculated through this polynomial. One way to make such an approximation is the Lagrange interpolation method, with which the n -sampling-point approximation equation can be generalized as

$$\tilde{z}^{-1} = \sum_{i=1}^h a_i z^{-i}, \text{ with } a_i = \prod_{j=1, j \neq i}^h \frac{\tilde{T}_s - jT_s}{iT_s - jT_s} \quad (4)$$

where \tilde{z}^{-1} denotes a virtual sampling delay, \tilde{T}_s is the corresponding virtual variable sampling period, a_i is the Lagrange polynomial coefficients, and h is the approximation order, i.e., how many points are used in the approximation.

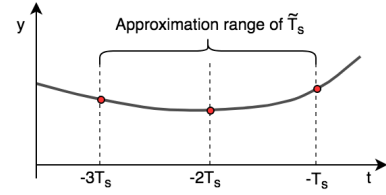


Fig. 5: Example of a variable sampling period approximation with 3 sampling points.

Clearly, a higher order approximation provides better accuracy and a wider range, while it also brings more computational burden. In this paper, the approximation order h is selected as 3, which ensures that the virtual variable sampling period \tilde{T}_s is able to be well approximated by the fixed sampling periods from T_s to $3T_s$. In the z -domain, this can be expressed as

$$\tilde{z}^{-1} = a_1 z^{-1} + a_2 z^{-2} + a_3 z^{-3}, \quad (5)$$

in which $a_1 = \frac{(\tilde{T}_s - 2T_s)(\tilde{T}_s - 3T_s)}{2T_s^2}$, $a_2 = \frac{(\tilde{T}_s - T_s)(\tilde{T}_s - 3T_s)}{-T_s^2}$, and $a_3 = \frac{(\tilde{T}_s - T_s)(\tilde{T}_s - 2T_s)}{2T_s^2}$.

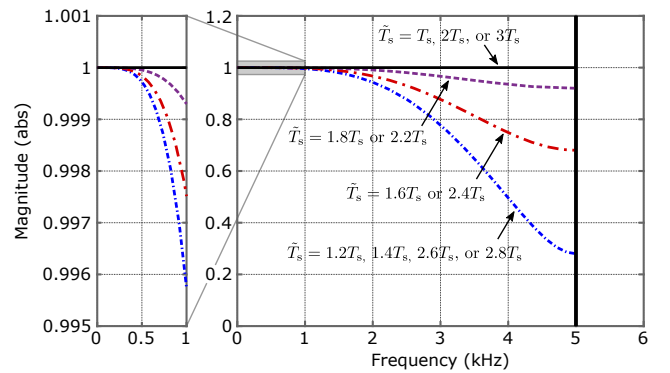


Fig. 6: Magnitude of the variable sampling period delay when the variable sampling period changes from T_s to $3T_s$.

To demonstrate the feasibility of this approximation, Fig. 6 shows the magnitude of a virtual variable delay unit \tilde{z}^{-1} using the 3-order Lagrange approximation when the VVS adaptive sampling period \tilde{T}_s changes from T_s to $3T_s$ under the sampling frequency of 10 kHz. From Eq. (4), the VVS adaptive delay unit $\tilde{z}^{-1} = z^{-1}$, z^{-2} , or z^{-3} , when the virtual sampling period $\tilde{T}_s = T_s$, $2T_s$, or $3T_s$, as shown in Fig. 6. There is no

approximation error obviously when $\tilde{T}_s = T_s, 2T_s$, or $3T_s$. The virtual variable delay unit performs as a low pass filter below the Nyquist frequency. For the low-frequency signal from 0 to 500 Hz, the virtual variable delay unit can approximate a real variable delay with an accuracy of above 99.97%, as observed in Fig. 6.

E. Frequency Adaptive VVS-SHRC

The virtual variable sampling approximation makes the SHRC frequency-adaptive. First, a proper constant sampling number N in one period is selected. Assuming that the reference period \tilde{T}_r fluctuates within the range $[T_{r_min}, T_{r_max}]$, and the virtual variable sampling period \tilde{T} has the range between T and $3T$, the constant sampling number N can be chosen as

$$\frac{T_{r_max}}{3nT} < N < \frac{T_{r_min}}{nT} \quad (6)$$

Normally, the constant sampling number N is chosen to be an integer near the middle of the range in Eq. (6) to allow the largest frequency adjustable range. With N being selected, the virtual variable sampling period \tilde{T}_s is set based on Eq. (3). When the period \tilde{T}_r of the reference signal varies, the virtual variable sampling period \tilde{T}_s adjusts accordingly to determine the virtual variable delay unit \tilde{z} . It is worth mentioning that the virtual variable delay unit is also flexible to realize fractional order phase lead compensation [8].

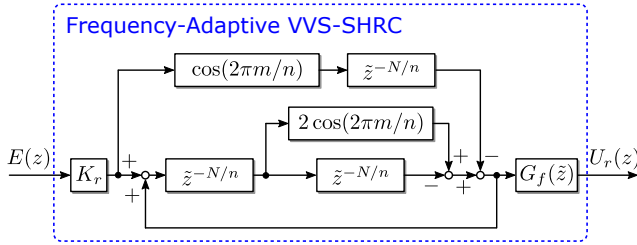


Fig. 7: Block diagram of the proposed FA-VVS-SHRC.

Replacing the fixed delay z^{-1} with the virtual variable delay \tilde{z}^{-1} , the transfer function of the FA-VVS-SHRC shown in Fig. 7 can be obtained as

$$G_{FA-VVS-SHRC}(\tilde{z}) = K_r \frac{[\cos(\frac{2\pi m}{n})\tilde{z}^{-\frac{N}{n}} - \tilde{z}^{-2\frac{N}{n}}]G_f(\tilde{z})}{1 - 2\cos(\frac{2\pi m}{n})\tilde{z}^{-\frac{N}{n}} + \tilde{z}^{-\frac{N}{n}}} \quad (7)$$

which does not require any hardware modifications, as aforementioned

III. EXPERIMENTS ON THREE-PHASE PWM INVERTERS

A. System modeling and state feedback controller

Fig. 8 shows a $(6k \pm 1)$ -order FA-VVS-SHRC controlled three-phase programmable PWM inverter, where E_n is the DC bus voltage, and L and C form a three-phase LC filter. The performance of the AC source is tested under a linear resistor load of R and a nonlinear rectifier load with diodes, capacitor C_r , and resistor R_r . The output voltage V_{ab} , V_{bc} , and V_{ca} , and inductor current I_{La} , I_{Lb} , and I_{Lc} are two states for a state feedback controller (SFC).

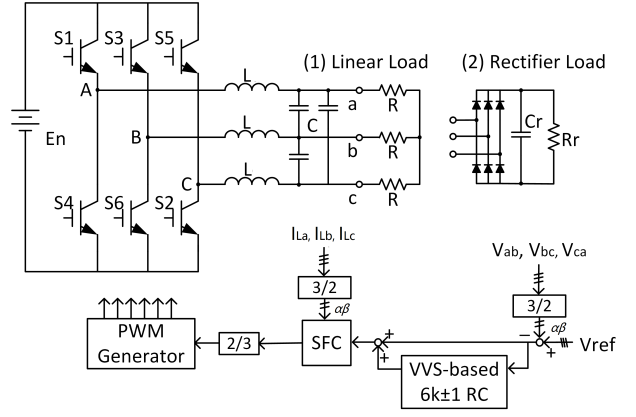


Fig. 8: Plug-in $(6k \pm 1)$ -order FA-VVS-SHRC controlled PWM inverter system.

The state space representation of the three-phase PWM inverter with the linear load in Fig. 8 is given as

$$\begin{aligned} \begin{bmatrix} 1 & 0 & -1 & 0 & 0 & 0 \\ -1 & 1 & 0 & 0 & 0 & 0 \\ 0 & -1 & 1 & 0 & 0 & 0 \\ 0 & 0 & 0 & 1 & -1 & 0 \\ 0 & 0 & 0 & 0 & 1 & -1 \\ 0 & 0 & 0 & -1 & 0 & 1 \end{bmatrix} \begin{bmatrix} \dot{v}_{ab} \\ \dot{v}_{bc} \\ \dot{v}_{ca} \\ i_{La} \\ i_{Lb} \\ i_{Lc} \end{bmatrix} &= \begin{bmatrix} \frac{-1}{2RC} & 0 & \frac{1}{2RC} & \frac{1}{C} & 0 & 0 \\ \frac{1}{2RC} & \frac{-1}{2RC} & 0 & 0 & \frac{1}{C} & 0 \\ 0 & \frac{1}{2RC} & \frac{-1}{2RC} & 0 & 0 & \frac{1}{C} \\ \frac{-1}{L} & 0 & 0 & 0 & 0 & 0 \\ 0 & \frac{-1}{L} & 0 & 0 & 0 & 0 \\ 0 & 0 & \frac{-1}{L} & 0 & 0 & 0 \end{bmatrix} \begin{bmatrix} v_{ab} \\ v_{bc} \\ v_{ca} \\ i_{La} \\ i_{Lb} \\ i_{Lc} \end{bmatrix} \\ &+ \begin{bmatrix} 0 & 0 & 0 \\ 0 & 0 & 0 \\ 0 & 0 & 0 \\ \frac{1}{L} & 0 & 0 \\ 0 & \frac{1}{L} & 0 \\ 0 & 0 & \frac{1}{L} \end{bmatrix} \begin{bmatrix} V_{AB} \\ V_{BC} \\ V_{CA} \end{bmatrix} \end{aligned} \quad (8)$$

where V_{AB} , V_{BC} and V_{CA} are the PWM voltages with values of either E_n or $-E_n$, and R, C, L are the load resistor, filter capacitor, and filter inductor of each phase [21].

When three-phase loads are balanced, Eq. (8) can be transformed into the $\alpha\beta$ -stationary reference frame [21] as

$$\begin{bmatrix} \dot{v}_\alpha \\ \dot{i}_\alpha \\ \dot{v}_\beta \\ \dot{i}_\beta \end{bmatrix} = \begin{bmatrix} \frac{-1}{3RC} & \frac{1}{3C} & 0 & 0 \\ \frac{1}{L} & 0 & 0 & 0 \\ 0 & 0 & \frac{-1}{3RC} & \frac{1}{3C} \\ 0 & 0 & \frac{1}{L} & 0 \end{bmatrix} \begin{bmatrix} v_\alpha \\ i_\alpha \\ v_\beta \\ i_\beta \end{bmatrix} + \begin{bmatrix} 0 & 0 \\ \frac{E_n}{L} & 0 \\ 0 & 0 \\ 0 & \frac{E_n}{L} \end{bmatrix} \begin{bmatrix} u_\alpha \\ u_\beta \end{bmatrix} \quad (9)$$

where state variables $v_\alpha, v_\beta, i_\alpha$, and i_β are the output voltages and the inductor currents in the $\alpha\beta$ -reference frame. The vector $[u_\alpha \ u_\beta]^T$ is the corresponding control vector. Eq. (9) can be treated as two independent systems with the same state space as [22]

$$\begin{bmatrix} v(k+1) \\ i(k+1) \end{bmatrix} = \begin{bmatrix} \varphi_{11} & \varphi_{12} \\ \varphi_{21} & \varphi_{22} \end{bmatrix} \begin{bmatrix} v(k) \\ i(k) \end{bmatrix} + \begin{bmatrix} g_1 \\ g_2 \end{bmatrix} u(k) \quad (10)$$

in which $v = v_\alpha$ or $v_\beta, i = i_\alpha$ or $i_\beta, u = u_\alpha$ or u_β , and the coefficients $\varphi_{11} = 1 - T_s/(3RC) + T_s^2/(18R^2C^2) - T_s^2/(6LC)$, $\varphi_{12} = T_s/(3C) - T_s^2/(18RC^2)$, $\varphi_{21} = -T_s/L + T_s^2/(6RLC)$, $\varphi_{22} = 1 - T_s^2/(6LC)$, $g_1 = E_n T_s^2/(6LC)$, $g_2 = E_n T_s/L$.

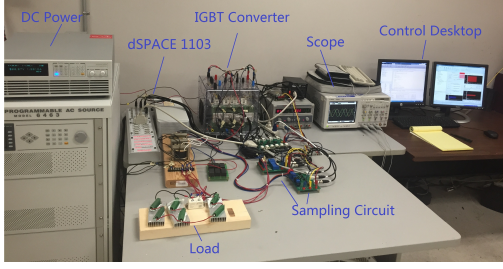


Fig. 9: Experimental platform of the three-phase inverter.

The SFC has the form of

$$u = -k_1 v(k) - k_2 i(k) + g v_{ref}(k) \quad (11)$$

where k_1, k_2 and g are the SFC parameters, v_{ref} is the reference sinusoidal voltage. With the SFC in Eq. (11), the transfer function can be rewritten as

$$G(z) = \frac{m_1 z + m_2}{z^2 + p_1 z + p_2} \quad (12)$$

with $p_1 = -(\varphi_{22} - g_2 k_2) - (\varphi_{11} - g_1 k_1)$, $p_2 = (\varphi_{11} - g_1 k_1)(\varphi_{22} - g_2 k_2) - (\varphi_{12} - g_1 k_2)(\varphi_{21} - g_2 k_1)$, $m_1 = g_1 k$, $m_2 = g_2 k - g_1 k(\varphi_{22} - g_2 k_2)$ [22]. The above SFC is then implemented in an experimental setup.

TABLE I: System Parameters.

Parameter	Value	Parameter	Value
DC voltage, E_n	400 V	Inductor, L	3 mH
Capacitor, C	10 μ F	PWM frequency	10 kHz
Sampling frequency, f_s	10 kHz	Linear load, R	200 Ω
Rectifier capacitor C_r	60 μ F	Rectifier inductor L_r	3 mH
Rectifier resistance R_r	200 Ω		

Fig. 9 shows the experimental platform. The SFC and RC schemes are designed in MATLAB Simulink, which are then loaded and implemented on a dSPACE DS1103 control board to control the PWM IGBT three-phase inverter. Table I lists the system parameters. Referring to Eq. (12) and Table I, the system transfer function is obtained as

$$G(z) = \frac{0.5971z + 0.0058}{z^2 - 0.8116z} \quad (13)$$

which indicates that the SFC system has poles at 0 and 0.81, implying that the system is stable. With only the feedback controller, there is a severe phase lag and the output waveform shows high distortions under both linear and rectifier load conditions, as shown in Fig. 10. Due to the structure of the 6-pulse commutation, the major distortion components appear at frequencies of $6k \pm 1$ times of the fundamental frequency, as observed in the harmonic analysis in Fig. 10 (the bottom ones).

Fig. 11 shows the Bode plots of the SFC and SFC with an RC. As the RC with a low pass filter provides identical compensation on all harmonics, there will be certain impact around crossover frequencies. This impact will limit the RC gain design range.

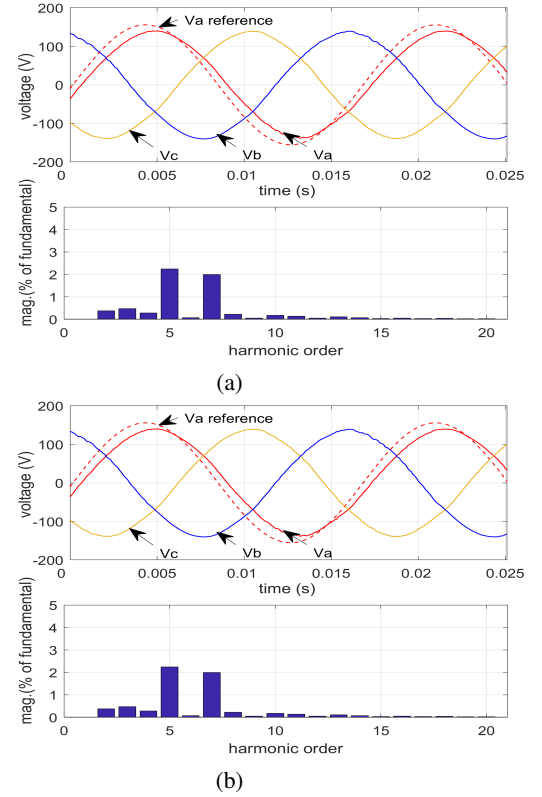


Fig. 10: Steady-state of the three-phase inverter with the SFC under (a) the linear load and (b) the nonlinear load.

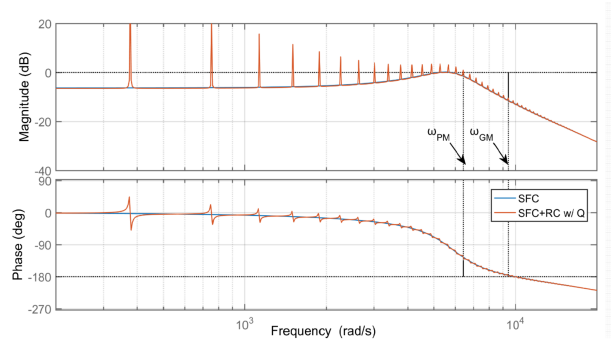


Fig. 11: Bode plot of the state feedback control with a repetitive control.

B. $(6k \pm 1)$ -order FA-VVS-SHRC

With the reference signal frequency $f_r = 60$ Hz ($T_r = 1/60$ s) and the sampling frequency $f_s = 10$ kHz ($T_s = 0.1$ ms), the delay length N is selected as 84, which is an integer multiple of $n = 6$. The adaptive delay unit is obtained from Eq. (4) as

$$\tilde{z}^{-1} = 0.0081z^{-1} + 0.9997z^{-2} - 0.0078z^{-3} \quad (14)$$

The next step is to choose the RC gain K_r and to build the linear phase-lead filter $G_f(\tilde{z})$. In this case, K_r is selected as 0.5 to achieve fast dynamics after applying the $(6k \pm 1)$ -order FA-VVS-SHRC. Note that $G_f(\tilde{z})$ will be used to compensate for not only the phase lag of the system model but also the unmodeled delays in the system. The phase lead of $G_f(\tilde{z})$

is designed following the analysis in [23], by measuring the actual system phase lag. The final phase lead is selected as

$$G_f(\tilde{z}) = \tilde{z}^{2.2} \approx -0.048\tilde{z}^1 + 0.864\tilde{z}^2 + 0.216\tilde{z}^3 - 0.032\tilde{z}^4 \quad (15)$$

C. Experimental validation

1) *Transient responses*: Fig. 12 shows the transient response and tracking error when the proposed $(6k \pm 1)$ -order FA-VVS-SHRC is applied to (a) the linear load and (b) the rectifier load, referring to Fig. 8. When the system operates with only the SFC, the peak tracking error is about 40 V due to the severe phase lag and magnitude error. After the $(6k \pm 1)$ -order FA-VVS-SHRC is put into use, the tracking error converges effectively and becomes stable within about 5-6 cycles or 0.1-0.12 seconds, as shown in Fig. 12.

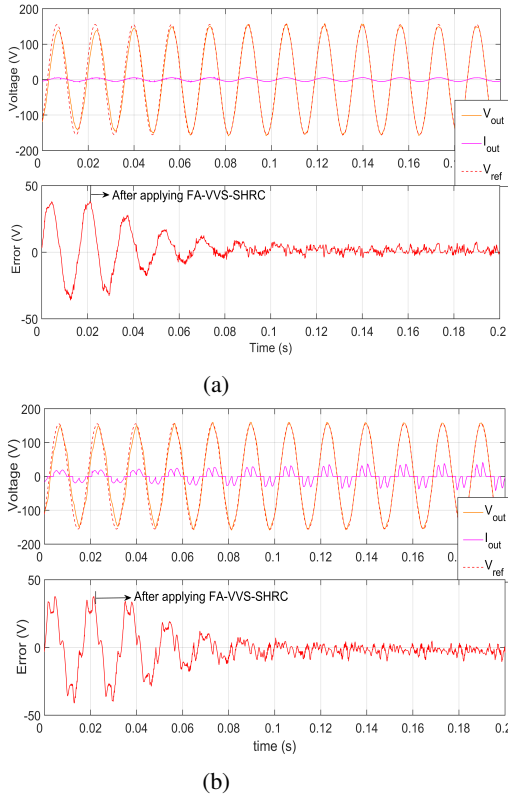


Fig. 12: Transient response of the three-phase inverter with the FA-VVS-SHRC (a) the linear load, (b) the nonlinear load.

2) *Steady-state responses*: Figs. 13 and 14 compare the steady-state performance of the three-phase $(6k \pm 1)$ -order SHRC without and with the frequency adaptive scheme under (a) the linear load and (b) the rectifier load. Comparing with the SFC performance in Fig. 10, the major distortion that locates at $(6k \pm 1)$ -order harmonics have been eliminated with the SHRC. However, Fig. 13 shows that the SHRC cannot achieve an accurate steady tracking because of the inaccuracy of the delay length of N/n . This is addressed by the precise phase compensation offered by the proposed virtual variable sampling approximation, as presented in Fig. 14. It is

observed in Fig. 14 shows that the $(6k \pm 1)$ -order FA-VVS-SHRC provides the most accurate voltage tracking and the least distortion.

TABLE II: Steady State Performance Comparison at 60Hz.

		SFC	SHRC	FA-VVS-SHRC
Linear Load	RMSE	23.77 V	5.43 V	2.59 V
	THD	2.34%	3.22%	1 %
Rectifier Load	RMSE	26.62 V	5.94 V	3.27 V
	THD	6.17%	4.11%	2.02 %

The PWM inverter steady-state performance is further assessed quantitatively by the root mean square tracking error (RMSE) and THD. Table II summarizes and compares the steady-state performance of the SFC, the conventional SHRC, and the FA-VVS-SHRC. The conventional SHRC under the linear and the rectifier loads yields the tracking errors of 5.43 V and 5.94 V, and the THD of 3.22% and 4.11%, respectively.

With the FA-VVS-SHRC, the tracking errors have 52.3% and 44.9% improvement over that of the conventional SHRC under the linear and the rectifier loads, and the THD improvement is 68.9% and 50.9%, respectively.

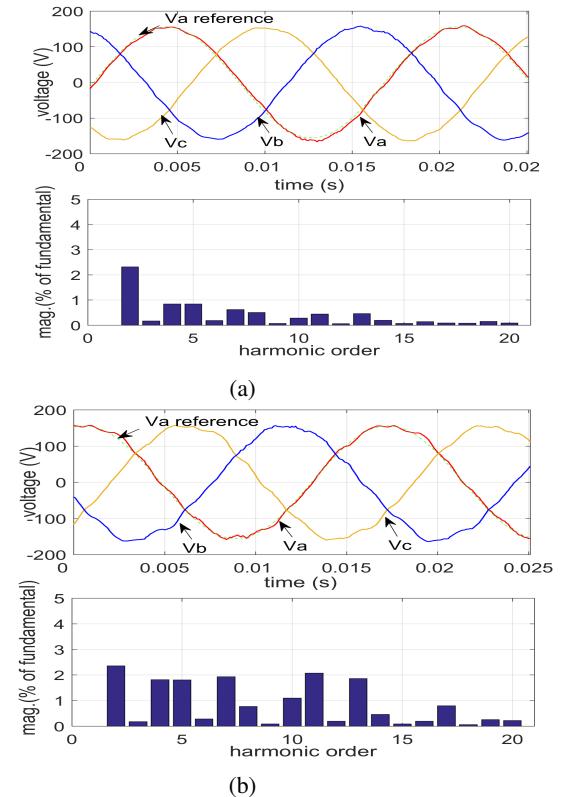


Fig. 13: Steady-state of the three-phase inverter with the conventional SHRC (a) the linear load, (b) the rectifier load.

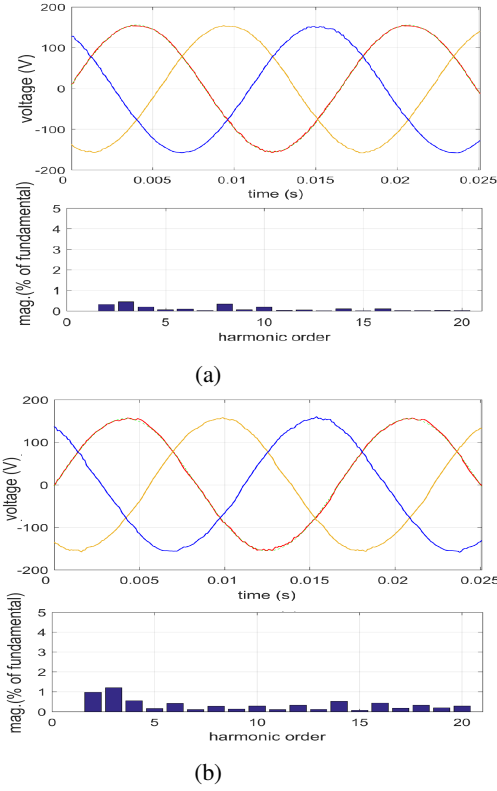


Fig. 14: Steady-state of three-phase inverter with the FA-VVS-SHRC (a) the linear load, (b) the rectifier load.

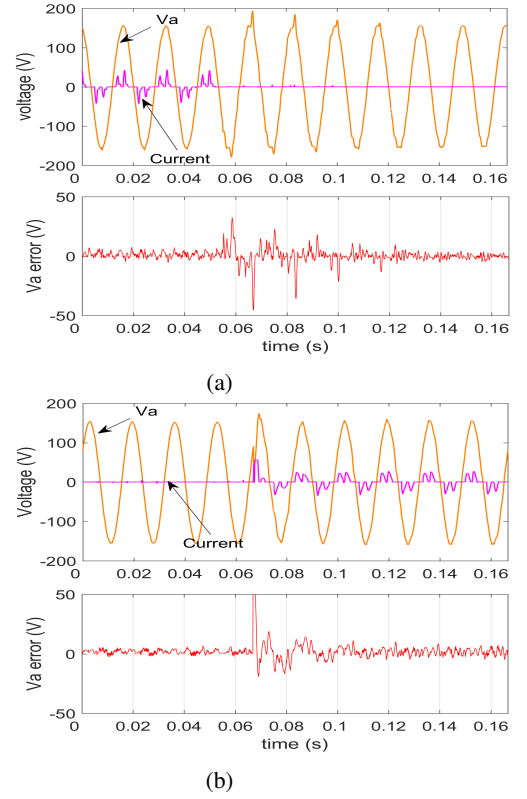


Fig. 16: Sudden load change (rectifier load and no load) with the proposed FA-VVS-SHRC.

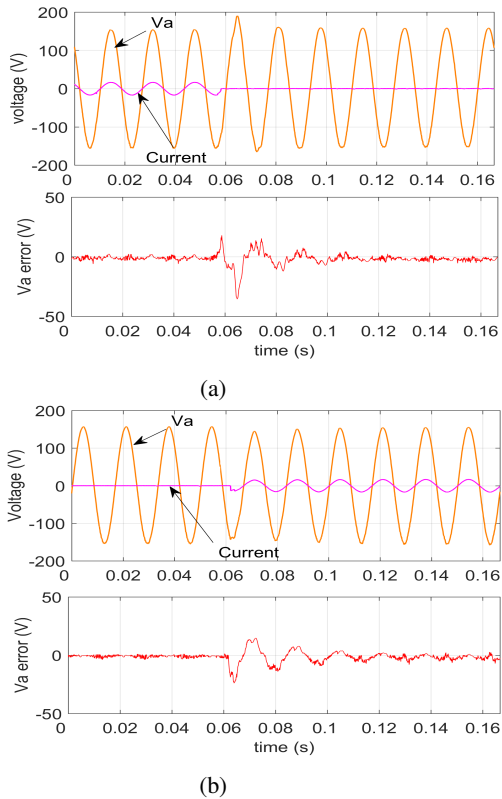


Fig. 15: Sudden load change (linear load and no load) with the proposed FA-VVS-SHRC.

3) *Sudden load change responses:* To further demonstrate the effectiveness of the FA-VVS-SHRC, Figs. 15 and 16 show the performance of the three-phase inverter under a load sudden change. The output voltage recovers to the steady state with limited tracking errors after several cycles fluctuation. The robustness of the proposed FA-VVS-SHRC is then verified based on the experimental tests.

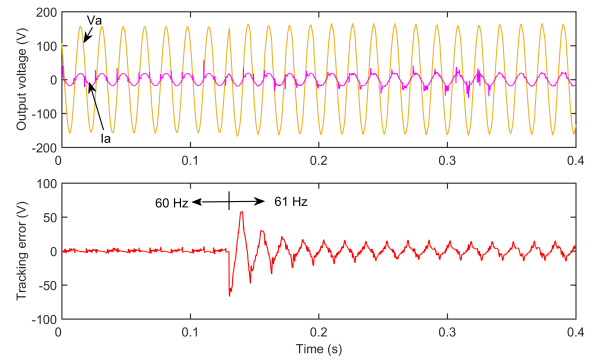


Fig. 17: Conventional SHRC under a linear load with frequency fluctuation (60 Hz to 61 Hz).

4) *Frequency change responses:* Figs. 17 and 18 show the transient response comparison of the conventional SHRC and the FA-VVS-SHRC when the reference frequency fluctuates. When the reference frequency changes from 60 Hz to 61 Hz, the FA-VVS-SHRC achieves 1.02 % THD and 2.63 V RMS tracking error after a certain transient process. On the contrary, the RMS tracking error and the THD of the conventional

SHRC are 6.80 V and 3.11 % when it reaches the steady state. Table III summarizes the results, which show that the proposed FA-VVS-SHRC can accommodate the disturbance from frequency fluctuations.

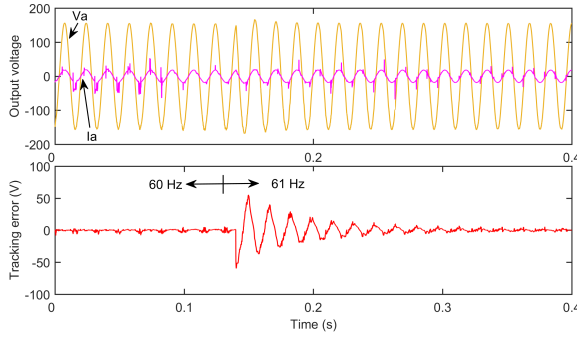


Fig. 18: FA-VVS-SHRC under a linear load with frequency fluctuation (60 Hz to 61 Hz).

TABLE III: Steady State Performance Comparison at 61 Hz.

	SHRC	FA-VVS-SHRC
RMSE	6.80 V	2.63V
THD	3.11%	1.02 %

IV. CONCLUSION

A frequency adaptive virtual variable sampling-based selective harmonic repetitive control (FA-VVS-SHRC) scheme is proposed in this paper to provide a tailor-made solution to compensate for harmonics produced by power inverters. The proposed FA-VVS-SHRC scheme offers a generic solution to the selective harmonic RC with high control accuracy guaranteeing strong robustness, enabling flexible fractional phase lead compensation, and being feasible for implementation in the presence of the fractional ratio of the sampling frequency to the fundamental reference frequency or time-varying reference frequency. Experiments on a three-phase power inverter under different load conditions, frequency fluctuations, sudden load changes have demonstrated the effectiveness of the proposed solution. The proposed FA-VVS-SHRC method can also be applied to other RCs and fractional phase delay compensation.

REFERENCES

- [1] G. Escobar, M. Hernandez-Gomez, A. A. Valdez-Fernandez, M. J. Lopez-Sanchez, and G. A. Catzin-Contreras, "Implementation of a $6n \pm 1$ repetitive controller subject to fractional delays," *IEEE Transactions on Industrial Electronics*, vol. 62, no. 1, pp. 444–452, Jan 2015.
- [2] K. Zhou, K.-S. Low, D. Wang, F.-L. Luo, B. Zhang, and Y. Wang, "Zero-phase odd-harmonic repetitive controller for a single-phase PWM inverter," *IEEE Transactions on Power Electronics*, vol. 21, no. 1, pp. 193–201, Jan 2006.
- [3] P. Mattavelli and F. P. Marafao, "Repetitive-based control for selective harmonic compensation in active power filters," *IEEE Transactions on Industrial Electronics*, vol. 51, no. 5, pp. 1018–1024, Oct 2004.
- [4] R. Costa-Castello, R. Grino, and E. Fossas, "Odd-harmonic digital repetitive control of a single-phase current active filter," *IEEE Transactions on Power Electronics*, vol. 19, no. 4, pp. 1060–1068, July 2004.

- [5] L. Jiang and D. Costinett, "A triple active bridge DC-DC converter capable of achieving full-range ZVS," in *Applied Power Electronics Conference and Exposition (APEC)*, 2016 IEEE, 2016, pp. 872–879.
- [6] M. Liserre, R. Teodorescu, and F. Blaabjerg, "Multiple harmonics control for three-phase grid converter systems with the use of pi-res current controller in a rotating frame," *IEEE Transactions on power electronics*, vol. 21, no. 3, pp. 836–841, 2006.
- [7] T. Roinila, H. Abdollahi, S. Arrua, and E. Santi, "Online measurement of bus impedance of interconnected power electronics systems: Applying orthogonal sequences," in *2017 IEEE Energy Conversion Congress and Exposition (ECCE)*, 2017, pp. 5783–5788.
- [8] Z. Liu, B. Zhang, and K. Zhou, "Universal fractional-order design of linear phase lead compensation multirate repetitive control for PWM inverters," *IEEE Transactions on Industrial Electronics*, vol. 64, no. 9, pp. 7132–7140, Sept 2017.
- [9] W. Lu, K. Zhou, D. Wang, and M. Cheng, "A generic digital $nk \pm m$ -order harmonic repetitive control scheme for PWM converters," *IEEE Transactions on Industrial Electronics*, vol. 61, no. 3, pp. 1516–1527, March 2014.
- [10] D. Chen, J. Zhang, and Z. Qian, "An improved repetitive control scheme for grid-connected inverter with frequency-adaptive capability," *IEEE Transactions on Industrial Electronics*, vol. 60, no. 2, pp. 814–823, Feb 2013.
- [11] Y. Yang, K. Zhou, H. Wang, F. Blaabjerg, D. Wang, and B. Zhang, "Frequency adaptive selective harmonic control for grid-connected inverters," *IEEE Transactions on Power Electronics*, vol. 30, no. 7, pp. 3912–3924, July 2015.
- [12] F. D. Freijedo, A. G. Yepes, J. Malvar, O. Lopez, P. Fernandez-Comesana, A. Vidal, and J. Doval-Gandoy, "Frequency tracking of digital resonant filters for control of power converters connected to public distribution systems," *IET Power Electronics*, vol. 4, no. 4, pp. 454–462, April 2011.
- [13] Z. X. Zou, K. Zhou, Z. Wang, and M. Cheng, "Frequency-adaptive fractional-order repetitive control of shunt active power filters," *IEEE Transactions on Industrial Electronics*, vol. 62, no. 3, pp. 1659–1668, March 2015.
- [14] M. A. Herran, J. R. Fischer, S. A. Gonzalez, M. G. Judewicz, I. Carugati, and D. O. Carrica, "Repetitive control with adaptive sampling frequency for wind power generation systems," *IEEE Journal of Emerging and Selected Topics in Power Electronics*, vol. 2, no. 1, pp. 58–69, March 2014.
- [15] P. Zanchetta, M. Degano, J. Liu, and P. Mattavelli, "Iterative learning control with variable sampling frequency for current control of grid-connected converters in aircraft power systems," *IEEE Transactions on Industry Applications*, vol. 49, no. 4, pp. 1548–1555, July 2013.
- [16] Z. Liu, B. Zhang, K. Zhou, and J. Wang, "Virtual variable sampling discrete fourier transform based selective odd-order harmonic repetitive control of DC/AC converters," *IEEE Transactions on Power Electronics*, vol. 33, no. 7, pp. 6444–6452, 2017.
- [17] Z. Liu, B. Zhang, K. Zhou, Y. Yang, and J. Wang, "Virtual variable sampling repetitive control of single-phase DC/AC PWM converters," *IEEE Journal of Emerging and Selected Topics in Power Electronics*, vol. 7, no. 3, pp. 1837–1845, 2019.
- [18] E. Kurniawan, Z. Cao, and Z. Man, "Design of robust repetitive control with time-varying sampling periods," *Industrial Electronics, IEEE Transactions on*, vol. 61, no. 6, pp. 2834–2841, June 2014.
- [19] J. Olm, G. Ramos, and R. Costa-Castello, "Stability analysis of digital repetitive control systems under time-varying sampling period," *IET control theory & applications*, vol. 5, no. 1, pp. 29–37, 2011.
- [20] Z. Liu, B. Zhang, and K. Zhou, "Virtual delay unit based digital $nk \pm m$ -order harmonic repetitive controller for PWM converter," in *Industrial Technology (ICIT)*, 2017 IEEE International Conference on. IEEE, 2017, pp. 248–253.
- [21] K. Zhou and D. Wang, "Digital repetitive controlled three-phase PWM rectifier," *Power Electronics, IEEE Transactions on*, vol. 18, no. 1, pp. 309–316, Jan 2003.
- [22] Z. Liu, B. Zhang, and K. Zhou, "Fractional-order phase lead compensation for multi-rate repetitive control on three-phase PWM DC/AC inverter," in *2016 IEEE Applied Power Electronics Conference and Exposition (APEC)*, March 2016, pp. 1155–1162.
- [23] B. Zhang, D. Wang, K. Zhou, and Y. Wang, "Linear phase lead compensation repetitive control of a CVCF PWM inverter," *IEEE Transactions on Industrial Electronics*, vol. 55, no. 4, pp. 1595–1602, April 2008.



Zhichao Liu (S'16) received his B.E and M.E. degrees in electrical engineering from East China University of Science and Technology, China, in 2008 and 2011, and Ph.D. degree in electrical engineering from University of South Carolina, SC, USA, in 2019.

Dr. Liu is currently with QCraft AI, working on motion planner and control algorithm design of autonomous vehicles. From 2008 to 2011, he was with Shanghai Baosight software, Co., Ltd. Shanghai, China. His research interest includes advanced control theory and applications, motion planner algorithm, digital control of power converter, and autonomous driving.



Yongheng Yang (SM'17) received the B.Eng. degree in electrical engineering and automation from Northwestern Polytechnical University, Shaanxi, China, in 2009 and the Ph.D. degree in electrical engineering from Aalborg University, Aalborg, Denmark, in 2014.

He was a postgraduate student with Southeast University, China, from 2009 to 2011. In 2013, he spent three months as a Visiting Scholar at Texas A&M University, USA. Currently, he is an Associate Professor with the Department of Energy Technology, Aalborg University, where he also serves as the Vice Program Leader for the research program on photovoltaic systems. His current research is on the integration of grid-friendly photovoltaic systems with an emphasis on the power electronics converter design, control, and reliability.

Dr. Yang is the Chair of the IEEE Denmark Section. He serves as an Associate Editor for several prestigious journals, including the IEEE Transactions on Industrial Electronics, the IEEE Transactions on Power Electronics, and the IEEE Industry Applications Society (IAS) Publications. He is a Deputy Editor of the IET Renewable Power Generation for Solar Photovoltaic Systems. He was the recipient of the 2018 IET Renewable Power Generation Premium Award and was an Outstanding Reviewer for the IEEE Transactions on Power Electronics in 2018.



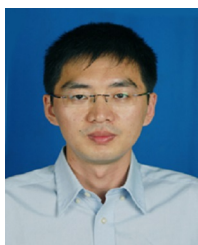
Bin Zhang (SM'08) received the B.E. and M.E. degrees from Nanjing University of Science and Technology, Nanjing, China, in 1993 and 1999, respectively, and the Ph.D. degree in Electrical Engineering from Nanyang Technological University, Singapore, in 2007.

Before he joined the Department of Electrical Engineering, University of South Carolina, Columbia, SC, USA, he was with General Motors R&D, Detroit, MI; Impact Technologies, Rochester, NY; and Georgia Institute of Technology, Atlanta, GA, USA. He has published over 100 technical papers. His current research interests include prognostics and health management, intelligent systems and controls, and their applications to various engineering systems.



Jingcheng Wang received the B.S. and M.S. degrees from Northwestern Polytechnical University, Xi'an, China, in 1993 and 1995, respectively, and the Ph.D. degree from Zhejiang University, Hangzhou, China, in 1998.

He is currently a Professor with Shanghai Jiaotong University, Shanghai, China. His current research interests include robust control, intelligent control, real-time control, and simulation.



Kelian Zhou (M'04–SM'08) received the B.Sc. degree from the Huazhong University of Science and Technology, Wuhan, China, in 1992, the M.Eng. degree from Wuhan Transportation University (now the Wuhan University of Technology), Wuhan, in 1995, and the Ph.D. degree in electrical engineering from Nanyang Technological University, Singapore, in 2002.

Currently, he is a full Professor with the School of Automation, Wuhan University of Technology. He has been a Senior Lecturer with the James Watt School of Engineering, University of Glasgow, Glasgow, U.K., during 2014–2020. He has authored or co-authored one monograph on Periodic Control of Power Electronic Converters, more than 120 technical papers, and several granted patents in relevant areas. His current research interests include power electronics and electric drives, renewable sources assessment and integration, and general PID control and applications.